Microstructure and Corrosion Behavior of Cold-Sprayed Zn-Al Composite Coating

Zhipo Zhao [1,2]**, Junrong Tang** [1,2]**, Naeem ul Haq Tariq** [3]**, Jiqiang Wang** [1,*]**, Xinyu Cui** [1] **and Tianying Xiong** [1,*]

[1] Shi-changxu Innovation Center for Advanced Materials, Institute of Metal Research, Chinese Academy of Science, Shenyang 110016, China; zpzhao16b@imr.ac.cn (Z.Z.); jrtang16s@imr.ac.cn (J.T.); xycui@imr.ac.cn (X.C.)

[2] School of Materials Science and Engineering, University of Science and Technology of China, Shenyang 110016, China

[3] Department of Metallurgy and Materials Engineering, Pakistan Institute of Engineering and Applied Sciences, Nilore, Islamabad 45650, Pakistan; NAEEM421@hotmail.com

[*] Correspondence: jqwang11s@imr.ac.cn (J.W.); tyxiong@imr.ac.cn (T.X.)

check for updates

Abstract: A Zn–Al composite coating was successfully deposited on Q235 steel by cold spray technology for the corrosion protection in the marine atmosphere. The microstructure and corrosion behavior of the prepared coating was studied byScanning Electron Microscope (SEM), X-ray Diffraction (XRD), salt spray test and electrochemical experiments. A 2400-h neutral salt spray corrosion test (with a corrosion medium of 3.5% sodium chloride solution) showed that the prepared cold-sprayed Zn-Al composite coating has excellent anti-corrosion properties. Based on the microstructure evolution and corrosion products analysis, droplets' flow-driven 'synergistic corrosion effect' was proposed to explain the co-corrosion behavior of Zn and Al particles in the composite coating.

Keywords: Zn–Al; composite coating; cold spray; salt spray test; corrosion

1. Introduction

Corrosion of maritime transport and offshore facilities is considered an issue of grave concern for the researchers due to huge economic and material losses [1–4]. Owing to its cheap cost and relatively superior properties (like strength, toughness, hardness, weldability, etc.), Q235 steel finds a spectrum of structural applications in the marine industry. However, in the marine environment, Q235 steel components suffer severe corrosion attack due to multiple factors that include temperature, the pH of sea water, light, micro-organisms, etc. Consequently, the mechanical properties of the alloy are severely degraded. This finally results in the premature failure of the engineering components, thus causing a high repairing cost as well as unscheduled downtime. The traditional ways of corrosion protection, like painting, do no work for Q235 steel due to its poor paint/substrate interfacial bonding. Therefore, it is of paramount importance to develop protective coatings for steel components for the long-term corrosion protection of steel components used in the marine environment [5–7].

Metallic protective coatings (especially Al and Zn coatings) play an important role for the corrosion protection of steel. Al coating can protect steel for a long time because of the existence of passivating film [8,9]. However, once the passivating film is damaged, it will lead to a serious pitting problem [10]. Zn coating is widely used in industry, which can not only prevent steel from corrosion, but also serve as a sacrificial anode to protect steel when the local coating is destroyed [11,12]. Therefore, Zn–Al composite coating combines the advantages of Zn and Al coating. This means it can not only isolate the corrosion medium for a long time, but also provides great galvanic protection as a sacrificial anode when the coating is damaged [10,13,14].

Thermal spray technologies, such as high-velocity oxygen-fuel (HVOF) spray [15,16], flame spraying [17,18] and arc spray [7,19,20] are the most common techniques to prepare Zn and Al coatings. However, due to the high process temperature of these techniques, the thermal-sprayed coatings inevitably have problems such as oxidation, phase transition, porosity and residual thermal stresses. For example, the porosity of arc spraying and flame spraying is generally higher than 10%, while plasma spraying and HVOF technologies usually results in 3–8% and <3% porosity, respectively [21,22]. Consequently, the quality of coatings is degraded due to the high porosity [23,24]. As an emerging solid-state deposition technology, cold spraying (CS) can avoid the abovementioned problems because the process temperature in the CS process remains well below the melting point of the raw feedstock materials [25–27]. In CS, metallic powders are accelerated by high-pressure gas to attain a supersonic speed, and then ballistically impacted on the substrate to form coatings due to their severe plastic deformation [28–30]. The cold-sprayed coatings are usually dense with a small porosity [31,32]. In general, the porosity of CS coatings can be less than 1% or even less than 0.3% when using optimized CS parameters or employing an situ shot peening strategy [33,34]. Therefore, CS is an excellent technology to fabricate dense metal-based coatings with relatively better corrosion resistance when compared with the coatings fabricated by thermal spray or other traditional coating technologies. Moreover, low-pressure CS provides an additional advantage of on-site repairing of worn out/unserviceable coatings or engineering components. In short, a CS of Zn–Al composite coating has considerable prospects for the protection of steel components used in marine environments. Therefore, different types of cold-sprayed Zn–Al composite coatings have been reported in the recent year, wherein researchers have mainly studied the microstructure and corrosion resistance of the coating. To our knowledge, limited research has been carried out to study the interaction between the two phases of the Zn–Al composite coating in the corrosion process [35,36].

This study was carried out with the aim to fabricate a viable protective coating for Q235 steel components used in marine environment and understand the corrosion mechanism of the prepared Zn–Al composite coating during assimilation with a marine environment. In this work, a Zn–Al composite coating was successfully deposited on commercial-grade Q235 steel by cold spray technology using mechanically mixed pure Al and Zn powders. To save cost, compressed air was used as the main gas as well as the powder-feeding gas. The microstructure and corrosion behavior of the prepared coating was studied in detail, and a synergistic corrosion effect of Zn and Al phases were proposed through the identification and analysis of corrosion products.

2. Materials and Methods

2.1. Substrate and Raw Powder Materials

In this work, a commercial-grade Q235 mild steel plate with dimensions $50 \times 100 \times 2$ mm^3 was used as the substrate. The chemical composition of the substrate is shown in Table 1. Commercial-grade pure Zn and Al powders were used as the feedstock for fabricating the Zn-Al composite coating. As shown in the scanning electron microscopy (SEM) images in Figure 1, both kinds of powders have a spherical morphology. The literature suggests that spherical powder is more suitable for cold spraying due to its good fluidity which often result in the coatings with lower porosity [37,38]. It is obvious in Figure 1 that Zn powder has a size range of 10–30 μm while Al powder has a bigger size range of 40–70 μm. Figure 1c shows the Back-Scattered Electron (BSE) detector image and the Energy Dispersive X-ray Spectroscopy (EDX) results of the mechanically mixed Zn–Al powders. It can be seen that, after mechanical mixing, the two powders are mixed evenly. Zn has a higher density than that of Al; therefore, it is relatively more difficult to accelerate Zn particles than Al particles with the same size. Therefore, using Zn powders with a smaller size can reduce the velocity difference between the two kinds of powders and improve the co-deposition efficiency of the raw powders [39,40].

Table 1. Composition of the mild steel.

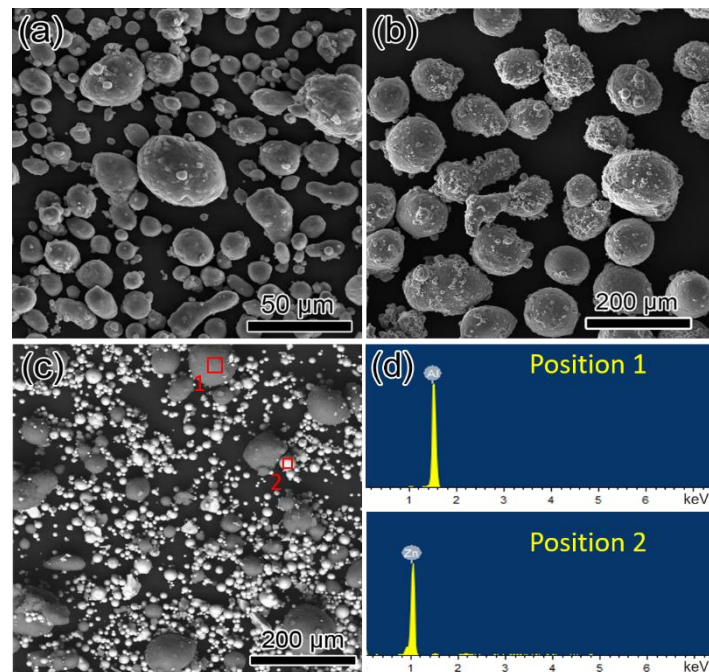| Element	Fe	C	Mn	Si	S	P
Content (wt.%)	balance	0.173	0.465	0.287	0.036	0.027

Figure 1. The Scanning Electron Microscopy (SEM) images of the as-received powders: (**a**) Zn powders; (**b**) Al powders; (**c**) Zn-Al mechanically mixed Zn–Al powders and (**d**) the EDX results of the region marked in (**c**).

2.2. Cold Spray Process

The Zn and Al powders with equal weight proportion (1:1) were mechanically mixed in a mixing barrel for 1 h. Based on the densities of Zn and Al, the volume fraction of Al powder in the mechanically mixed raw powders was calculated to be 73%. Before the experiment, the Q235 steel substrate was sand blasted to remove the oxidation layer, roughen the surface, and obtain a fresh surface with high surface energy. An in-house, high-pressure CS facility was used. A rectangular de Laval-type nozzle, with the length of 130 mm, a throat size of 2×3 mm^2, and an outlet size of 2×20 mm^2 was used for CS. The parameters of CS have great influence on the quality of the coating. For metallic powders, increasing the main gas pressure and heating temperature may result in sufficient deformation of the particles which in turn results in lower porosity in the coatings. However, the high temperature causes the particles to soften up, resulting in nozzle clogging [41]. After performing a series of preliminary experiments, the following optimized CS parameters were used to obtain dense Zn–Al coating with good quality. Compressed air was used as the main gas as well as the powder-feeding gas to save cost. The pressure of the main gas was 2.0 MPa while its temperature was 300 °C. The powder-feeding gas pressure was 2.3 MPa and the powder feeding rate was 15 g/min. The stand-off distance between the nozzle and the substrate was constantly fixed to 20 mm. The substrate was fixed, and the spray nozzle was moved by using a KUKA robot (KUKA, Augsburg, Germany). During CS, the nozzle was moved at Z-shaped line, and the moving distance between each pass was 4 mm.

2.3. Coating Characterization

The compositions of different phases of the coating were investigated by X-ray diffraction system (XRD, PHILIPS-X'Pert MPD, Eindhoven, The Netherlands) using Cu K_α radiation with the scan

rate of 0.04°/s. The microstructure and composition of the Zn–Al composite coating was studied by scanning electron microscopy (SEM, ZEISS, ULTRA PLUS, Jena, Germany) equipped with an Energy Dispersive X-ray Spectroscopy (EDX ZEISS, ULTRA PLUS, Jena, Germany) system. The SEM images were analyzed using Image J software (ImageJ 1.52a, national institutes of health, Bethesda, MD, USA).

In order to evaluate the corrosion resistance of the as-sprayed Zn–Al coating, electrochemical experiments were carried out in a three-electrode flask full of 3.5 wt.% sodium chloride solutions, with a saturated potassium chloride electrode as the reference electrode, a platinum as the counter electrode and a sample with area of 1 cm^2 as the working electrode. The measurement range of Tafel polarization curve was −0.5 to +0.5 V (based on open circuit potential, OCP), and the scanning rate was 0.33 mV/s.

Further, salt spray corrosion tests were carried out in a salt spray chamber (Qingdao Jingke Detection equipment co., Ltd., JK-600, Qingdao, China). For the salt spray corrosion test, 3.5 wt.% sodium chloride solutions with pH ranging from 6.8 to 7.2 were used. Each test lasted for 200 days at a temperature of 34–36 °C. The evolution of the Zn–Al composite coating surface was recorded with the help of a digital camera, and the corrosion products were carefully analyzed by XRD and SEM.

3. Results and Discussion

Figure 2 shows the microstructure of the as-sprayed Zn–Al coating at different magnifications. It can be observed in Figure 2a that the thickness of the cold-sprayed coating is 640 μm, and the coating bonds well with the substrate, with no visible pores or cracks. The backscattered SEM image clearly reveals intermixed Zn particles (gray zone) and Al particles (black zone). Both kinds of particles are evenly distributed throughout the coating. This indicates that the mechanical mixing method is desirable for achieving uniform composite coating. Image J software was used to analyze the fraction of Zn and Al phases in the coating. The results showed that the fraction of Al in the cross-sectional micrograph is 70.08%, which is basically the same as the fraction of Al powders in the raw mixed powders (73%). Considering the calculation error, this confirms that the deposition efficiencies of the two kinds of metal powders are basically the same. Figure 2b reveals that Zn and Al particles underwent severe plastic deformation during high-speed impact, which resulted flattened particles and waterfall-like pattern. Moreover, small particles (as marked by green arrows in Figure 2b) can be observed at the two poles of the deformed particles. These tiny particles are the splashed debris formed during high speed impact.) Figure 2c shows a high-magnification microphotograph of the composite coating. Discontinuous pores (marked by yellow arrows) can be found between the splat boundaries, which are less than 2 μm in length and less than 0.5 μm in width. Image J software analysis indicated that the porosity of the Zn–Al coating was only 0.4%. This suggests better corrosion resistance of the prepared cold-sprayed coating when compared with thermal-sprayed coatings with much higher porosity [7].
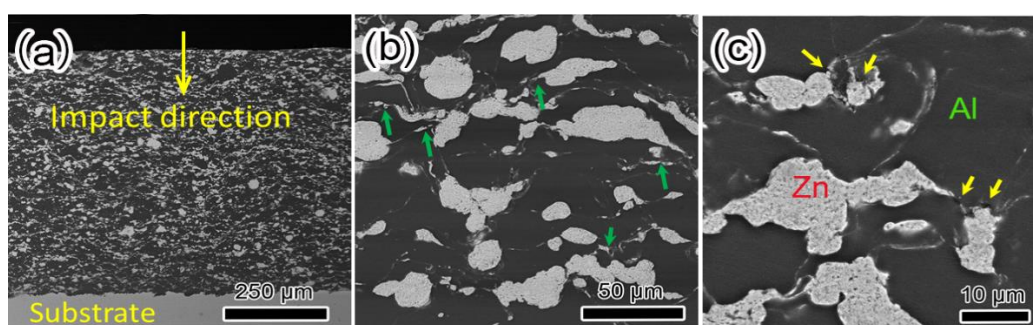

Figure 2. The Backscattered SEM images of as-sprayed Zn–Al coating at (**a**) 250×; (**b**) 500× and (**c**) 3000× magnification.

To investigate the corrosion behavior of Zn–Al composite coating, the polarization curves of as-sprayed Zn–Al composite coatings, pure Zn coating and pure Al coating were measured in 3.5% NaCl solutions. The polarization curves of the samples are shown in Figure 3, and the results are summarized in Table 2. It can be seen in Figure 3 that the corrosion potential of the Zn–Al composite coating (-1.12 V_{SCE}) falls between pure Al coating (-1.00 V_{SCE}) and Zn coating (-1.27 V_{SCE}). In general, for the sacrificial anode coatings, the more negative the corrosion potential, the better the protective ability of the coating. Further, the corrosion current of the Zn–Al coating (0.77 $\mu A/cm^2$) is nearly two times higher than that of pure Al coating (0.32 $\mu A/cm^2$) but nearly five times lower than that of pure Zn coating (3.80 $\mu A/cm^2$). Smaller corrosion current means lower corrosion rate, so the Zn–Al composite coating shows a corrosion rate of 0.39 mpy, nearly four times lower than that of Zn coating. This indicates that the Zn–Al coating combines the advantages of pure Zn coating and pure Al coating. As a protective coating for steel, the cold-sprayed Zn–Al coating not only shows good cathodic protection through sacrificial anodic action, but also has a low corrosion rate, which is beneficial for long-term corrosion protection.
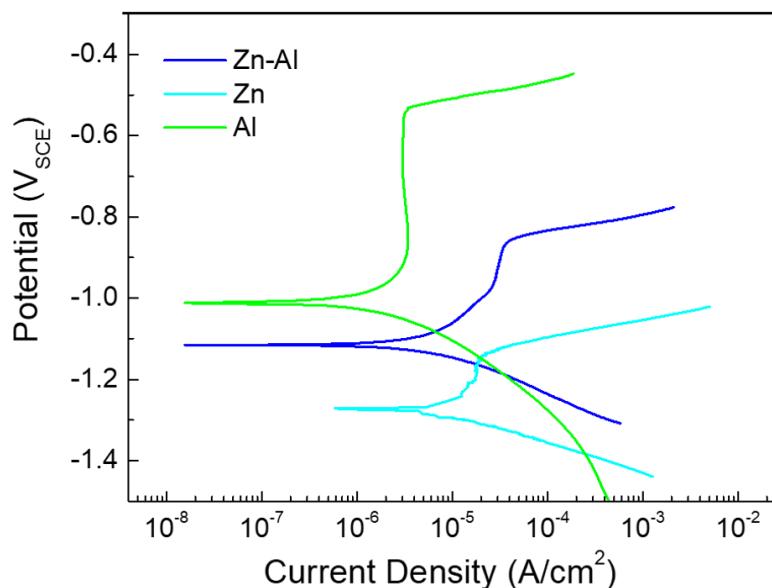

Figure 3. The potentiodynamic polarization curves of as-sprayed Zn–Al coating, Al coating and Zn coating.

Table 2. Results of potentiodynamic polarization test in 3.5 wt.% NaCl solution.

Sample	E_{corr} (V_{SCE})	I_{corr} ($\mu A/cm^2$)	E_{pit} (V_{SCE})	Corrosion Rate (mpy)
Al	-1.00	0.32	-0.54	0.18
Zn	-1.27	3.80	-1.15	1.64
Zn-Al	-1.12	0.77	-0.86	0.39

Figure 4 shows the surface evolution of the Zn–Al composite coating during a 200-day salt spray corrosion test. The as-sprayed coating shows a smooth surface with no visible defect. After 10 days of the salt spray corrosion test, white rust spots began to appear on some local areas. With the passage of time, the number of white rust spots gradually increased. When the salt spray corrosion test lasted for 50 days, the white rust area covered almost 50% of the surface of the composite coating. After 100 days, loose and porous corrosion products began to appear at the edges of the coating. When the corrosion products were removed by a soft brush, few shallow pits were revealed out. After 150 days, pits appeared at the central region of the sample and covered whole area of the coating. There were more corrosion products formed near the edges of the sample when the salt spray test lasted for 200 days. It is worth noting that no red rust was formed even after 200 days, indicating that the Zn–Al composite coating has a good corrosion resistance for low-carbon steel substrates.
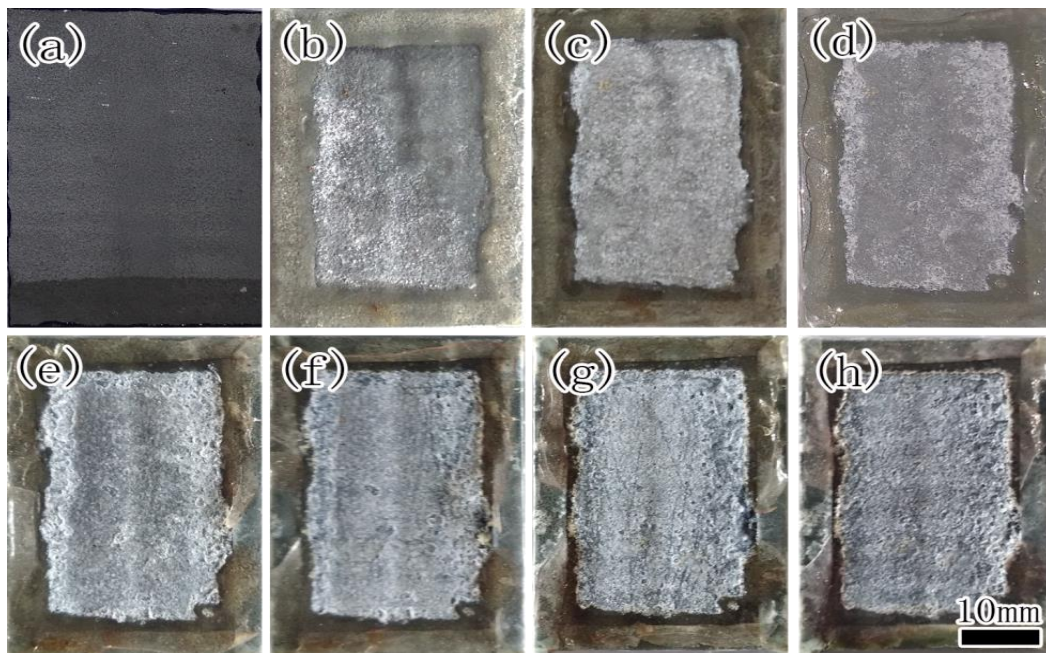
Figure 4. The optical photographs of the composite coating during salt spray test after (**a**) 0 days; (**b**) 10 days; (**c**) 15 days; (**d**) 25 days; (**e**) 50 days; (**f**) 100 days; (**g**) 150 days; (**h**) 200 days.

Figure 5 shows the cross-sectional micrographs of the Zn–Al composite coating after a 200-day salt spray corrosion test. There is a clear separation line (highlighted by red dotted line) between the corroded area and the uncorroded area of the coating. At the bottom of the coating, the uncorroded area retained the initial microstructure of the as-sprayed composite coating, as shown in Figure 2. Further, the corroded area of the coating is parallel to the substrate, indicating uniform corrosion attack instead of local corrosion. This indicates that the mixed Zn–Al coating can improve the resistance against pitting. In this kind of corrosion mode, the service time of the coating is proportional to its thickness. This infers that we can improve the service time of the coating by depositing a thicker coating. Moreover, the shielding effect of the corrosion products would retard the permeation of the corrosive medium. Considering the potential of CS for preparing thick metallic coatings [25], it would not be difficult to prepare a thick, cold-sprayed Zn–Al coating for long-term corrosion resistance in marine environment. Figure 5c shows the top area of the corroded coating. The yellow arrows highlight the pitting pores, around which loose corrosion products can be seen. The green arrows highlight the needle-like corrosion products, which will be discussed in detail later.
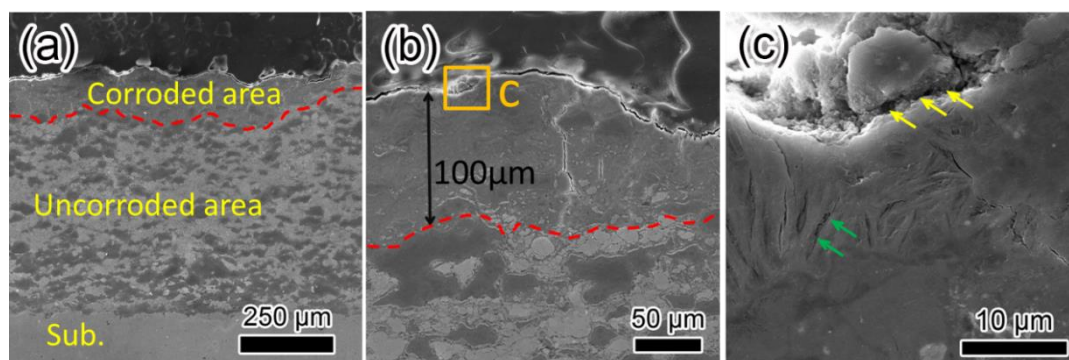

Figure 5. The SEM images of cross-section micrographs of the coating after 200 days of the salt spray corrosion test at (**a**) 250×; (**b**) 500× and (**c**) 3000× magnification.

Figure 6 shows the XRD patterns of as-sprayed Zn–Al composite coating (curve "a") and the corroded coating after 200 days of salt spray corrosion test (curve "b"). It is quite clear that curve (a) contains the characteristic diffraction peaks of pure Zn and Al, indicating that no obvious oxidation or phase transition has taken place during the CS process. In contrast, the XRD pattern of the salt-sprayed Zn–Al composite coating shows complex features. After matching the relevant JCPDF cards for XRD, phases like $Zn_6Al_2(OH)_{16}CO_3 \cdot 4H_2O$, $Zn_5(OH)_8Cl_2 \cdot H_2O$, $Zn_5(CO_3)_2(OH)_6$, ZnO and Al_2O_3 were identified as the corrosion products in Zn–Al composite coating. These are the typical corrosion products which have been reported in the literature for Zn–Al coatings being used in marine environment [12,17,42]. Among these corrosion products, basic carbonates (such as $Zn_6Al_2(OH)_{16}CO_3 \cdot 4H_2O$ and $Zn_5(CO_3)_2(OH)_6$) could form dense protective layer. This results in effective sealing of the pores to prevent penetration of corrosive media deep into the coating.
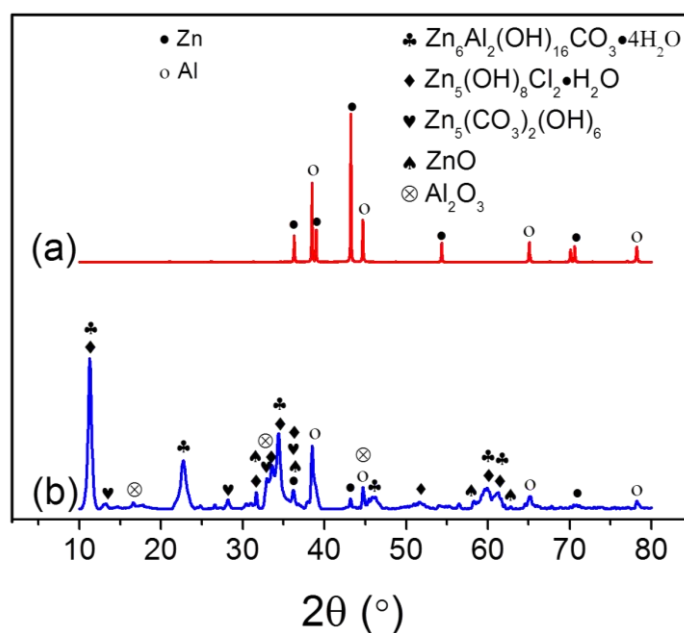

Figure 6. The XRD patterns of as-sprayed Zn-Al composite coating (**a**) and the corroded coating (**b**).

To understand the corrosion mechanism, the morphology and composition of the corrosion products were investigated by SEM and EDS. Figure 7 shows the morphologies of corrosion products of the salt-sprayed sample after 200 days. After the corrosion of Zn–Al composite coating, the surface on the coating was filled with cracks and loose corrosion products were formed. These corrosion products were quite different from those of the as-sprayed coating. Some typical corrosion products were selected in Figure 7a for further investigation. Figure 7b shows formation of few insular debris through the cracking of oxide layers. The EDS results indicated that the main components of the insular debris are Zn, Al, O and C. Combining EDS and XRD results, it is speculated that the insular debris is $Zn_6Al_2(OH)_{16}CO_3 \cdot 4H_2O$. Figure 7c,d show some interlaced flaky corrosion products. Further, EDS results confirmed that the flaky corrosion products consist of Zn, Cl, and O. Combined with the XRD pattern (b), it can be inferred that the flaky corrosion product is $Zn_5(OH)_8Cl_2 \cdot H_2O$. Figure 7e shows some spherical corrosion products. The high-magnification image (Figure 7f) reveals that the spherical corrosion products are actually composed of the needle-like entities. It seems that these are the similar corrosion products which were observed in the SEM image of the 200-day salt-sprayed coating (i.e., needle-like corrosion products as marked by green arrows in Figure 5c). The EDS analysis revealed that these phases are composed of Zn, C, and O. Together with the XRD result, these phases were identified as $Zn_5(CO_3)_2(OH)_6$, the common initial corrosion products of Zn in the marine environment [12].
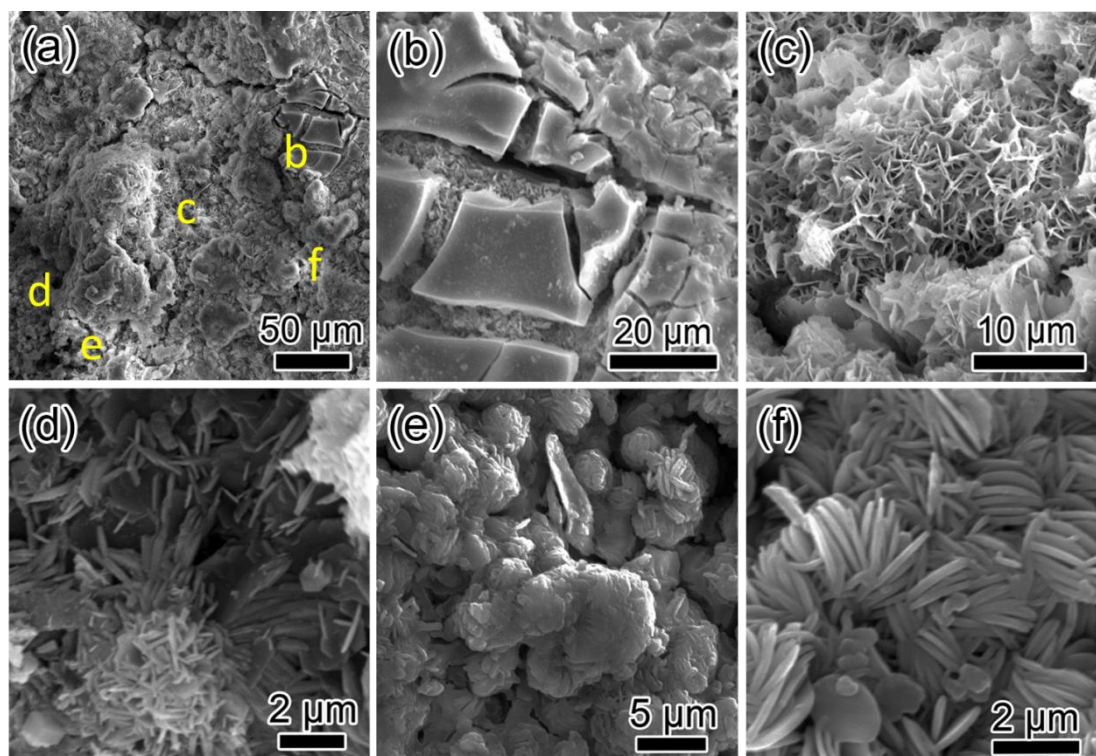
Figure 7. The morphologies of Zn–Al coating's corrosion products after a 200-day salt spray test: (**a**) macroscopic morphologies of the combined corrosion products, in which position b–f represent different corrosion products; (**b**) $Zn_6Al_2(OH)_{16}CO_3 \cdot 4H_2O$; (**c**) $Zn_5(OH)_8Cl_2 \cdot H_2O$; (**d**) high-magnification image of $Zn_5(OH)_8Cl_2 \cdot H_2O$; (**e**) $Zn_5(CO_3)_2(OH)_6$; (**f**) high-magnification image of $Zn_5(CO_3)_2(OH)_6$.

It is worth mentioning that the prepared cold-sprayed Zn–Al coating was formed without alloying using pure Zn and Al particles. However, plenty of Zn–Al compounds were found in the corrosion products. To explain this phenomenon, the droplets' flow-driven 'synergistic corrosion effect' is proposed as follows. Figure 8 shows a schematic diagram for the process of forming the Zn–Al compounds corrosion products. We assumed that, in the salt spray environment, there are many drops of salt solution sprayed on the coating. In the first phase, small droplets rich in Cl^- ions gather on the surface of metal particles, resulting in the formation of a localized oxygen concentration cell. Since the edge of the droplet is thin, it has a high oxygen concentration which facilitates a cathodic reaction at the edges. At cathodic regions, oxygen gets electrons and the hydroxyl ions are released, as shown in Figure 8. At the same time, carbon dioxide from the environment dissolves in the droplets and forms carbonate ions. An anodic region is formed in the middle of the droplets, where the oxygen concentration is lower wherein metal gets oxidized to produce metal ions. Driven by voltage, negatively charged ions such as hydroxyl ions move from the edge of the droplets to the middle of the droplets and finally combine with metal ions to form $Al(OH)_3$ or $Zn(OH)_2$. In the second phase, the droplets flow out and get inter-mixed. Consequently, some corrosion products formed in the first phase, such as $Zn_5(CO_3)_2(OH)_6$, $Zn_5(OH)_8Cl_2$ and metallic oxide (formed through dehydration of metallic hydroxide, are segregated on the surface). Since the mixed droplets contain Zn^{2+}, Al^{3+}, Cl^-, CO^{2-} and OH^- ions, these ions form compounds like $Zn_6Al_2(OH)_{16}CO_3$ and other corrosion products after a series of chemical reactions. In summary, there is a synergistic effect between the two kinds of phases (rather than separate corrosion of each other or simple galvanic corrosion) during the corrosion process of Zn–Al composite coating. The droplets flow on the surface of the coating, promoting the dissolution reaction of two different phases to occurs synchronously, inhibiting the pitting of either phase. This behavior is similar to uniform corrosion; therefore, the service life of the Zn–Al composite

coating to is proportional to its thickness. In other words, the service life of the composite coating can be predicted according to its thickness, which has high application significance.
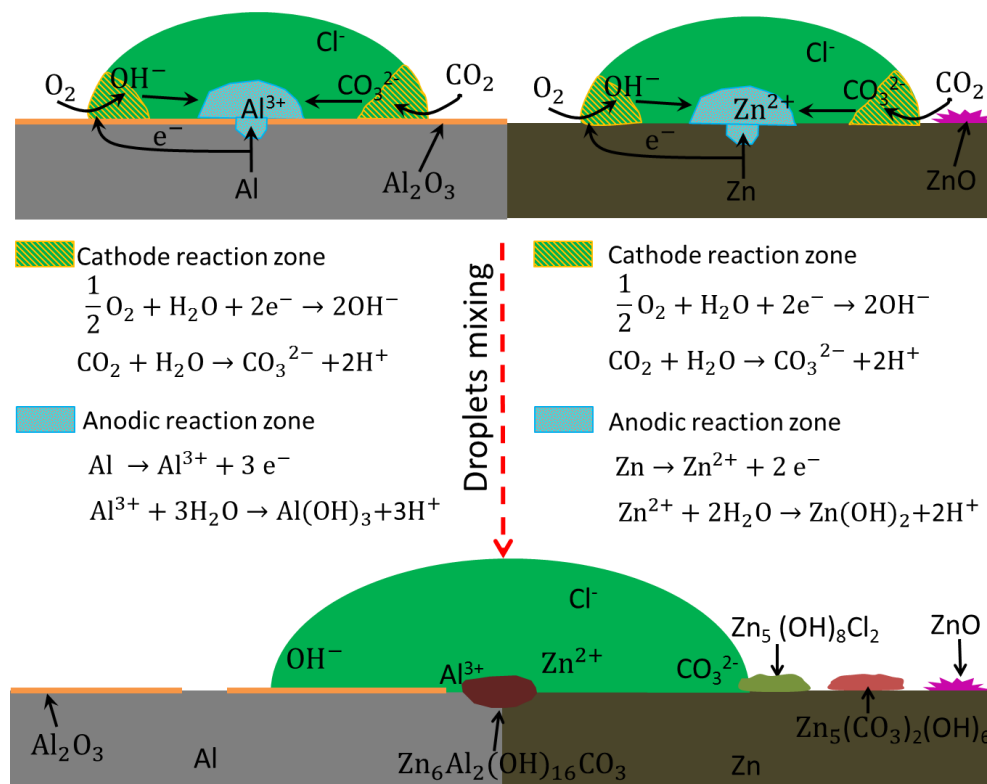

Figure 8. Diagram of the synergistic corrosion process of the Zn–Al composite coating.

4. Conclusions

In this paper, Zn–Al composite coating was successfully deposited on a commercial-grade Q235 steel substrate by cold spray using mechanically mixed Zn and Al powders. The microstructure and corrosion behavior of the coating were studied in detail. The following are the main conclusions of this study:

a.   The prepared cold-sprayed composite coating was dense with a porosity of 0.4%. Zn and Al phases were distributed uniformly in the composite coating;

b.   The composite coating showed uniform corrosion attack instead of local corrosion during the salt spray test, which is beneficial for achieving the long-term corrosion of the coating in marine environment;

c.   The main corrosion products of the Zn-Al composite coating were $Zn_6Al_2(OH)_{16}CO_3 \cdot 4H_2O$, $Zn_5(OH)_8Cl_2 \cdot H_2O$, $Zn_5(CO_3)_2(OH)_6$, ZnO and Al_2O_3;

d.   There was a synergistic corrosion effect between the Zn and Al phases, promoted by the flow of the droplets, which looks similar to uniform corrosion.

Author Contributions: Conceptualization, T.X., X.C.; methodology, Z.Z.; date analysis, Z.Z. and J.T.; data curation, Z.Z.; writing—original draft preparation, Z.Z.; writing—review and editing, J.T., N.u.H.T. and J.W. All authors have read and agreed to the published version of the manuscript.

References

1. Alcantara, J.; de la Fuente, D.; Chico, B.; Simancas, J.; Diaz, I.; Morcillo, M. Marine Atmospheric Corrosion of Carbon Steel: A Review. *Materials* **2017**, *10*, 406. [CrossRef] [PubMed]

2. Soares, C.G.; Garbatov, Y.; Zayed, A.; Wang, G. Influence of environmental factors on corrosion of ship structures in marine atmosphere. *Corros. Sci.* **2009**, *51*, 2014–2026. [CrossRef]

3. Ma, Y.; Li, Y.; Wang, F. The atmospheric corrosion kinetics of low carbon steel in a tropical marine environment. *Corros. Sci.* **2010**, *52*, 1796–1800. [CrossRef]

4. Adedipe, O.; Brennan, F.; Kolios, A. Review of corrosion fatigue in offshore structures: Present status and challenges in the offshore wind sector. *Renew. Sustain. Energy Rev.* **2016**, *61*, 141–154. [CrossRef]

5. Bala, N.; Singh, H.; Karthikeyan, J.; Prakash, S. Cold spray coating process for corrosion protection: A review. *Surf. Eng.* **2014**, *30*. [CrossRef]

6. Qian, Y.; Li, Y.; Jungwirth, S.; Seely, N.; Fang, Y.; Shi, X. The Application of Anti-Corrosion Coating for Preserving the Value of Equipment Asset in Chloride-Laden Environments: A Review. *Int. J. Electrochem. Sci.* **2015**, *10*, 10756–10780.

7. Moon, K.-M.; Kim, Y.-H.; Lee, M.-H.; Baek, T.-S. Polarization characteristics of four types of coating films by thermal spray in seawater solution. *Mod. Phys. Lett. B* **2015**, *29*. [CrossRef]

8. Niu, L.; Chang, S.-H.; Su, Y.; Han, D.; Li, G. A aluminum coating with chromium-free passivating film formed on AZ91D magnesium alloy. *J. Alloy. Compd.* **2015**, *635*, 11–15. [CrossRef]

9. Feliu, S., Jr.; Bartolome, M.J.; Gonzalez, J.A.; Lopez, V.; Feliu, S. Passivating oxide film and growing characteristics of anodic coatings on aluminium alloys. *Appl. Surf. Sci.* **2008**, *254*, 2755–2762. [CrossRef]

10. Bonabi, S.F.; Ashrafizadeh, F.; Sanati, A.; Nahvi, S.M. Structure and Corrosion Behavior of Arc-Sprayed Zn-Al Coatings on Ductile Iron Substrate. *J. Therm. Spray Technol.* **2018**, *27*, 524–537. [CrossRef]

11. Sajjadnejad, M.; Mozafari, A.; Omidvar, H.; Javanbakht, M. Preparation and corrosion resistance of pulse electrodeposited Zn and Zn-SiC nanocomposite coatings. *Appl. Surf. Sci.* **2014**, *300*, 1–7. [CrossRef]

12. Persson, D.; Thierry, D.; Karlsson, O. Corrosion and corrosion products of hot dipped galvanized steel during long term atmospheric exposure at different sites world-wide. *Corros. Sci.* **2017**, *126*, 152–165. [CrossRef]

13. Su, F.; Zhang, P.; Wei, D.; Chen, X.; Ding, F.; Wang, B. Corrosion behavior of hot-dip Al-Zn coating doped with Si, RE, and Mg during exposure to sodium chloride containing environments. *Mater. Corros. Werkst. Korros.* **2018**, *69*, 714–724. [CrossRef]

14. Su, X.; Zhou, J.; Wang, J.; Wu, C.; Liu, Y.; Tu, H.; Peng, H. Thermodynamic analysis and experimental study on the oxidation of the Zn-Al-Mg coating baths. *Appl. Surf. Sci.* **2017**, *396*, 154–160. [CrossRef]

15. Wood, R.J.K.; Speyer, A.J. Erosion-corrosion of candidate HVOF aluminium-based marine coatings. *Wear* **2004**, *256*, 545–556. [CrossRef]

16. Torres, B.; Taltavull, C.; Lopez, A.J.; Campo, M.; Rams, J. Al/SiCp and Al11Si/SiCp coatings on AZ91 magnesium alloy by HVOF. *Surf. Coat. Technol.* **2015**, *261*, 130–140. [CrossRef]

17. Katayama, H.; Kuroda, S. Long-term atmospheric corrosion properties of thermally sprayed Zn, Al and Zn-Al coatings exposed in a coastal area. *Corros. Sci.* **2013**, *76*, 35–41. [CrossRef]

18. De Rincon, O.; Rincon, A.; Sanchez, M.; Romero, N.; Salas, O.; Delgado, R.; Lopez, B.; Uruchurtu, J.; Marroco, M.; Panosian, Z. Evaluating Zn, Al and Al-Zn coatings on carbon steel in a special atmosphere. *Constr. Build. Mater.* **2009**, *23*, 1465–1471. [CrossRef]

19. Lee, H.S.; Ismail, M.A.; Choe, H.B. Arc thermal metal spray for the protection of steel structures: An overview. *Corros. Rev.* **2015**, *33*, 31–61. [CrossRef]

20. Yang, H.Q.; Yao, Z.J.; Wei, D.B.; Zhou, W.B.; Yin, G.X.; Feng, L.X. Anticorrosion of thermal sprayed Al-Zn-Si coating in simulated marine environments. *Surf. Eng.* **2014**, *30*, 801–805. [CrossRef]

21. Odhiambo, J.G.; Li, W.; Zhao, Y.; Li, C. Porosity and Its Significance in Plasma-Sprayed Coatings. *Coatings* **2019**, *9*, 460. [CrossRef]

22. Kawaguchi, Y.; Miyazaki, F.; Yamasaki, M.; Yamagata, Y.; Kobayashi, N.; Muraoka, K. Coating Qualities Deposited Using Three Different Thermal Spray Technologies in Relation with Temperatures and Velocities of Spray Droplets. *Coatings* **2017**, *7*, 27. [CrossRef]

23. Yin, S.; Chen, C.; Suo, X.; Lupoi, R. Cold-Sprayed Metal Coatings with Nanostructure. *Adv. Mater. Sci. Eng.* **2018**. [CrossRef]

24. Grujicic, M.; Zhao, C.L.; DeRosset, W.S.; Helfritch, D. Adiabatic shear instability based mechanism for particles/substrate bonding in the cold-gas dynamic-spray process. *Mater. Des.* **2004**, *25*, 681–688. [CrossRef]

25. Yin, S.; Cavaliere, P.; Aldwell, B.; Jenkins, R.; Liao, H.; Li, W.; Lupoi, R. Cold spray additive manufacturing and repair: Fundamentals and applications. *Addit. Manuf.* **2018**, *21*, 628–650. [CrossRef]

26. Gaertner, F.; Schmidt, T.; Stoltenhoff, T.; Kreye, H. Recent developments and potential applications of cold spraying. *Adv. Eng. Mater.* **2006**, *8*, 611–618. [CrossRef]

27. Champagne, V.; Helfritch, D. The unique abilities of cold spray deposition. *Int. Mater. Rev.* **2016**, *61*, 437–455. [CrossRef]

28. Schmidt, T.; Gartner, F.; Assadi, H.; Kreye, H. Development of a generalized parameter window for cold spray deposition. *Acta Mater.* **2006**, *54*, 729–742. [CrossRef]

29. Schmidt, T.; Assadi, H.; Gaertner, F.; Richter, H.; Stoltenhoff, T.; Kreye, H.; Klassen, T. From Particle Acceleration to Impact and Bonding in Cold Spraying. *J. Therm. Spray Technol.* **2009**, *18*, 794–808. [CrossRef]

30. Assadi, H.; Gartner, F.; Stoltenhoff, T.; Kreye, H. Bonding mechanism in cold gas spraying. *Acta Mater.* **2003**, *51*, 4379–4394. [CrossRef]

31. Moridi, A.; Hassani-Gangaraj, S.M.; Guagliano, M.; Dao, M. Cold spray coating: Review of material systems and future perspectives. *Surf. Eng.* **2014**, *30*, 369–395. [CrossRef]

32. Balani, K.; Laha, T.; Agarwal, A.; Karthikeyan, J.; Munroe, N. Effect of carrier gases on microstructural and electrochemical behavior of cold-sprayed 1100 aluminum coating. *Surf. Coat. Technol.* **2005**, *195*, 272–279. [CrossRef]

33. Zahiri, S.H.; Fraser, D.; Gulizia, S.; Jahedi, M. Effect of Processing Conditions on Porosity Formation in Cold Gas Dynamic Spraying of Copper. *J. Therm. Spray Technol.* **2006**, *15*, 422–430. [CrossRef]

34. Luo, X.-T.; Wei, Y.-K.; Wang, Y.; Li, C.-J. Microstructure and mechanical property of Ti and Ti6Al4V prepared by an in-situ shot peening assisted cold spraying. *Mater. Des.* **2015**, *85*, 527–533. [CrossRef]

35. Lu, X.; Wang, S.; Xiong, T.; Wen, D.; Wang, G.; Du, H. Anticorrosion Properties of Zn-Al Composite Coating Prepared by Cold Spraying. *Coatings* **2019**, *9*, 210. [CrossRef]

36. Haixiang, L.I.; Xiangbo, L.I.; Mingxian, S.U.N.; Hongren, W.; Guosheng, H. Corrosion resistance of cold-sprayed Zn-50Al coatings in seawater. *J. Chin. Soc. Corros. Prot.* **2010**, *30*, 62–66.

37. Wong, W.; Vo, P.; Irissou, E.; Ryabinin, A.N.; Legoux, J.G.; Yue, S. Effect of Particle Morphology and Size Distribution on Cold-Sprayed Pure Titanium Coatings. *J. Therm. Spray Technol.* **2013**, *22*, 1140–1153. [CrossRef]

38. Jodoin, B.; Ajdelsztajn, L.; Sansoucy, E.; Zúñiga, A.; Richer, P.; Lavernia, E.J. Effect of particle size, morphology, and hardness on cold gas dynamic sprayed aluminum alloy coatings. *Surf. Coat. Technol.* **2006**, *201*, 3422–3429. [CrossRef]

39. Li, H.; Sun, M.; Li, X.; Wang, H.; Huang, G. Depositing characteristic of 65% Zn-Al coatings produced by cold gas dynamic spray. *Chin. J. Nonferrous Met.* **2010**, *20*, 1353–1359.

40. Lou, K. The Organizational Structure of the Cold Spraying Al Composite Coating and Corrosion Behavior Research. Master's Thesis, JiMei University, Fujian, China, 2017.

41. Wang, X.; Zhang, B.; Lv, J.; Yin, S. Investigation on the Clogging Behavior and Additional Wall Cooling for the Axial-Injection Cold Spray Nozzle. *J. Therm. Spray Technol.* **2015**, *24*, 696–701. [CrossRef]

42. Cole, I.S.; Ganther, W.D.; Furman, S.A.; Muster, T.H.; Neufeld, A.K. Pitting of zinc: Observations on atmospheric corrosion in tropical countries. *Corros. Sci.* **2010**, *52*, 848–858. [CrossRef]